




## Research Article

# Optimization Process of Potassium Carbonate Activated Carbon through Jute-Based Core Materials by Using Artificial Neural Network with Response Surface Methodology

L. Natrayan <sup>1</sup>, V. R. Niveditha,<sup>2</sup> S. Kaliappan,<sup>3</sup> Pravin P. Patil,<sup>4</sup> C. K. Arvinda Pandian <sup>5</sup>,  
Y. Sessa Rao,<sup>6</sup> and P. Murugan <sup>7</sup>

<sup>1</sup>Department of Mechanical Engineering, Saveetha School of Engineering, SIMATS, Chennai, Tamil Nadu 602105, India

<sup>2</sup>Department of Computer Science and Engineering, Sathyabama Institute of Science and Technology, Chennai, 600119 Tamil Nadu, India

<sup>3</sup>Department of Mechanical Engineering, Velammal Institute of Technology, Chennai, 601204 Tamil Nadu, India

<sup>4</sup>Department of Mechanical Engineering, Graphic Era Deemed to be University, Bell Road, Clement Town, 248002 Dehradun, Uttarakhand, India

<sup>5</sup>Department of Automobile Engineering, School of Mechanical Sciences, B. S. Abdur Rahman Crescent Institute of Science & Technology, Vandalur, Chennai, 600048 Tamil Nadu, India

<sup>6</sup>Department of Mechanical Engineering, QIS College of Engineering and Technology, Ongole, Andhra Pradesh, India

<sup>7</sup>Department of Mechanical Engineering, Jimma Institute of Technology, Jimma University, Ethiopia

Correspondence should be addressed to P. Murugan; murugan.ponnusamy@ju.edu.et

Received 19 October 2022; Revised 25 December 2022; Accepted 5 April 2023; Published 17 April 2023

Academic Editor: Debabrata Barik

Copyright © 2023 L. Natrayan et al. This is an open access article distributed under the Creative Commons Attribution License, which permits unrestricted use, distribution, and reproduction in any medium, provided the original work is properly cited.

Potassium carbonate was tested as novel information for producing carbonaceous materials from jute cores. Two quadratic models have been developed for both answers to link the preparatory parameters: activating temperatures, molar ratio, and incubation time. The RSM and ANN models were used to improve the processing conditions to maximise the quantities of iodine and methylene blue penetration. The best charcoal was obtained using 900°C activating temperatures, a 1.5 molar ratio, and a 4-hour activating time. This resulted in iodine and methylene blue absorption of 1260.07 mg/g and 369.21 mg/g, respectively. It was discovered that the K<sub>2</sub>CO<sub>3</sub>-based pyrolysis process might be anticipated to become a safe yet incredibly efficient process of making activated carbons with a very well-defined and monocultural porous structure. Even though the precise emphasis given to K<sub>2</sub>CO<sub>3</sub> is unknown at the moment, given the creation of K<sub>2</sub>C<sub>3</sub>O<sub>4</sub> just after evolution with one additional molarity of CO at approximately 870°C, these same porous and papule responses begun by K<sub>2</sub>CO<sub>3</sub> stimulation might be temporarily posited to be quite comparable to an initiation action needed to make progress by K<sub>2</sub>C<sub>3</sub>O<sub>4</sub>. The influence of control parameters was examined in this study using variance analysis like the ANOVA test. Furthermore, the response surface (RSM) and artificial neural networks (ANN) are employed to improve the output results while optimising the methylene blue and iodine qualities. Consequently, the experimental findings correlate well with the statistics.

## 1. Introduction

Activated carbon is a flexible, highly porous concept widely used as an adsorbent in fluid and gas processes and heterogeneous catalysis. As contamination has become a much more significant issue, the demand for carbonaceous materials grows. The characteristics of carbonaceous materials

are determined by the activating agent's quality and activating techniques [1, 2]. In practice, anthracite, hardwood, and coconut husks are the historical documents of commercially carbonaceous materials. Owing to their cheap cost, durability, and ease of handling, several agricultural wastes have subsequently gained a lot of interest as alternate materials for manufacturing carbonaceous materials [3, 4].

Pollutants encircled humans, which appears to be a significant threat to all life forms. Developed countries attempt to reduce pollution by adopting drastic measures to substitute polluting resources with sustainable alternatives [5]. Scientists have developed an organic biobased alternative to the existing composite polymers. Composites are regarded as essential components in a wide range of large-scale operations [6]. Substantial expenditures were invested in developing synthetic composites that have functioned admirably in various uses. However, with increasing global warming and risks, significant attention has shifted to creating biological and nanocomposite materials [7]. Consequently, the production of such hybrids has received considerable attention in recent history. Biocomposites were already being researched to replicate the success of synthetic fibre. Such biocomposites are recyclable, and various natural fibres were employed in their creation to make them sustainable and environmentally friendly in origin, with fewer emissions [8, 9]. Compared to proprietary brands, the composite material has also gained popularity due to its excellent compressive and flexural qualities. Biocomposites are organic, compact, lightweight, emitting little CO<sub>2</sub>, and having minimal material and production costs. Above everything, the fibres employed in the production of biocomposites are plentiful in the environment. Because of their numerous practical uses, biocomposites are now on the verge of being intrinsic community members [10, 11].

Furthermore, jute fibres are environmentally benign, recyclable, inexpensive, and disposable. Jute fibres are mainly composed of lignocellulosic materials [12]. Cellulose is a polymer that aids in the presence of hydrogen among substrates with fibres, hence increasing interface contractures. Jute fibre is in significant demand outside the composites and biopolymer sectors [13]. Jute fibre qualities are often influenced by the tree's age, fibre content, and hybrid production procedures. Jute fibre is now employed in various industries, including fabrics, cars, and many uses [14]. Jute plant, also known as ligno, was used in the automotive industry to make a variety of components such as side panels, hatchback linings, and centre consoles. In particular, large automakers like Daimler, as well as numerous European and American automakers, are eager to incorporate increasingly sustainable composite and polymeric materials. Jute-based biocomposites comprising natural substances have evolved in recent years with excellent tensile qualities over native jute-based hybrids [15, 16].

Because jute core fibre has a considerably large lignin concentration but little coal ash, it is a suitable substrate for commercially generating quality charcoal filters to increase financial benefit [17]. Munawar et al. [8] reported the combustion accompanied by potassium iodide activation of jute matting to produce active carbon fibre (ACF) with the most excellent permeability of 582 m<sup>2</sup>/g. To the aim of contributing, published studies on the use of discarded jute cores for the generation of chemical activation are scarce [18]. Various activating processes are used in synthesising carbonaceous materials: physiological, chemical, and biophysical engagement. Carbonization has unique benefits, including solitary activation, higher production, and

TABLE 1: BBD constraints and their levels.

Sl. no	Parameters	L1	L2	L3
1	Impregnation ratio	1	1.5	2
2	Time (hrs)	3	3.5	4
3	Temperature (°C)	800	850	900

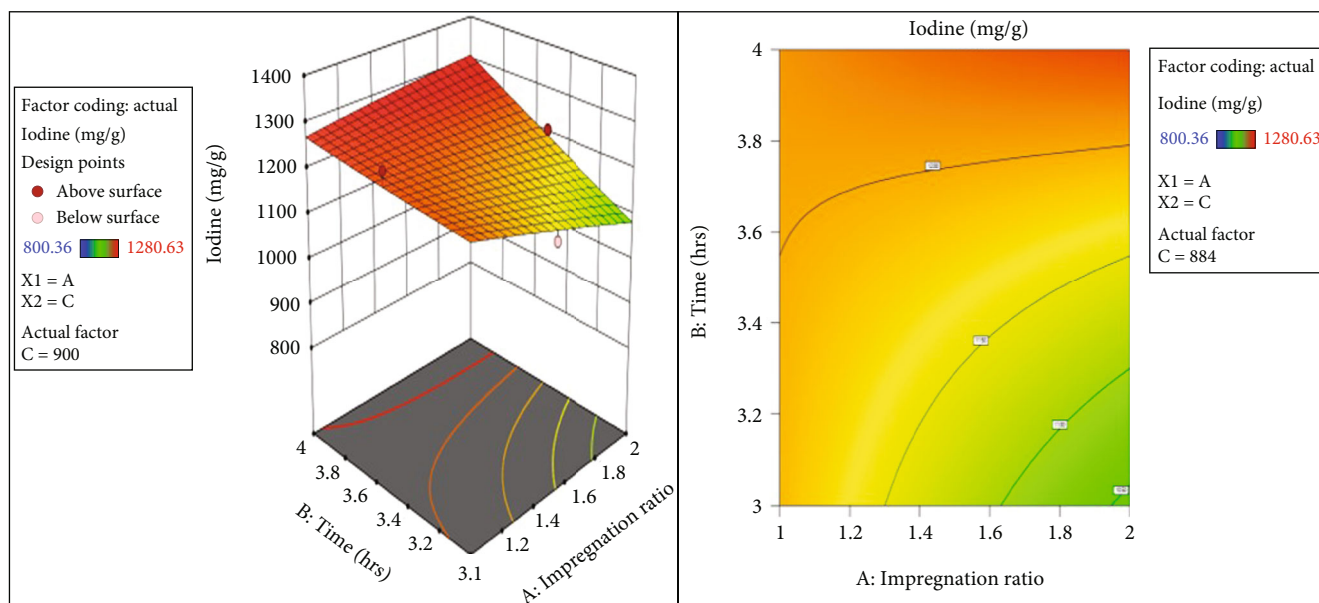
improved micropores [19]. The more powerful and successful molecular enhancers in manufacturing high surface energy carbonaceous materials are phosphoric acid, zinc chloride, potassium hydroxide, and potassium carbonate [20]. Potassium salts were discovered to be more effective activation chemicals than most in producing activated charcoal materials of high porosity and permeability values. Nonetheless, our understanding of carbonization pathways is far from complete [21, 22].

The Box-Behnken experimental setup for RSM and ANN were used to analyse the impact of important evaluation factors using potassium iodide and methylene blue adsorbent value systems as reactions to identify the most appropriate initiation method for creating jute-based charcoal filters to preferred adsorbent performance this season by K<sub>2</sub>CO<sub>3</sub> stimulation. In the proposed investigation, potassium carbonate has been used as an alternate efficient activating agent to manufacture jute-based chemical activation. This is because the iodine amount and adsorption isotherm values are the most commonly used metrics for accurately measuring the adsorption ability of the porous structure architectures of the carbon materials generated. On the other hand, the iodine number can be roughly comparable to the absorber plate area of a charcoal molecule in m<sup>2</sup>/g. As a result, the iodine number and the sorbent grade are commonly employed as adsorbed species indicators, exhibiting excellent significant associations with the adsorption process of sorbent material in small and medium-scale molecules separately. The outcomes of this study help generate a prospective new pharmacological activation and produce good use of jute to make charcoal filters have desirable characteristics by determining the ideal operating settings using RSM and ANN approaches.

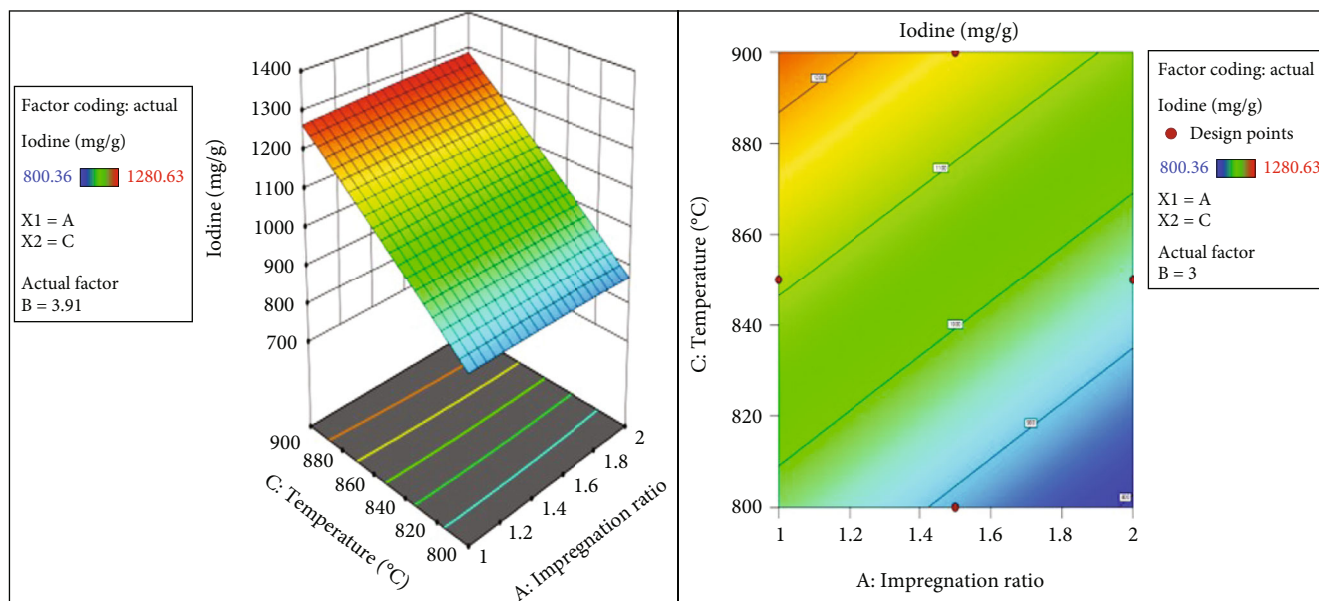
## 2. Investigational Works

*2.1. Materials.* The jute came from the Jute Research Farm Salam in Tamil Nadu, India. That production's chemical products were of analytical reagents. Before any additional interventions, the viscose cores were cleaned with water to eliminate impurities, dry at 110°C for 48 hours, and crushed; then, samples were filtered to 100-212 mesh size.

*2.2. Creation of Activated Carbon.* The research was conducted at various K<sub>2</sub>CO<sub>3</sub>/forerunner insemination concentrations. The 25g of dried precursors were steeped in a 25% K<sub>2</sub>CO<sub>3</sub> mixture at ambient atmospheric conditions for 14 hours, with periodic mixing. The mixture was then continuously dried in a hot oven at 110 degrees Celsius. This solvent temperature was increased to the specified ultimate heat in a burner at a fluid velocity of 350 mL/min of nitrogen. In addition, jute core carbon was made at 900°C for 3

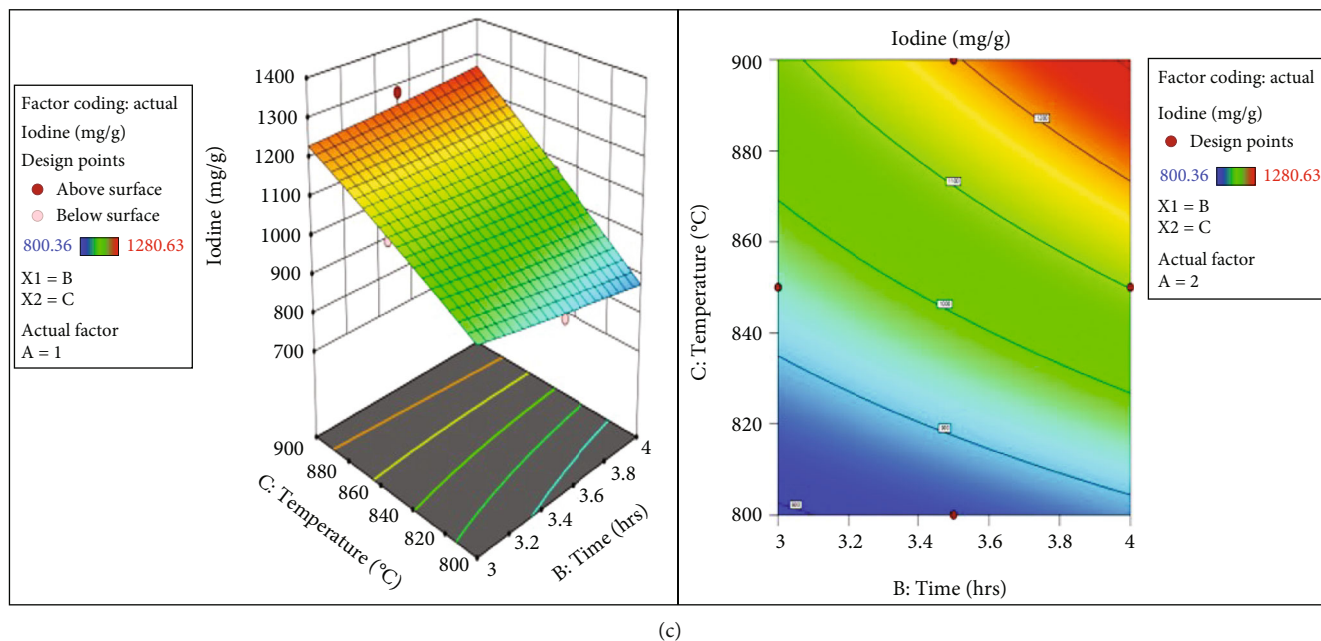


(a)



(b)

FIGURE 1: Continued.



(c)

FIGURE 1: Response 3D surface and contour plots of iodine number based on the input parameters.

hours before implantation using  $K_2CO_3$  solutions. The compounds were washed several times using 0.5 ml of hydrochloric acid with rubbing alcohol till the pH of a supernatant approached about 6.0, dried over 24 hours at  $110^\circ C$ , and then measured.

**2.3. Adsorption Characteristics.** Both the iodine amount and methylene blue adsorption have been measured in accordance with GB/T 12496.8-1999 and GB/T 12496.10-1999, respectively. Iodine is a typical absorption coefficient probing chemical, representing small pores with diameters greater than 1.0 nanometers. On the other hand, methylene blue is the most widely used modelling structure for evaluating an adsorbent's most significant potential to reduce soluble compounds with molecular sizes greater than 1.5 nanometers. The adsorbent capabilities of iodine and MB are provided in milligrammes of adsorbent surface captured by 1 gramme of charcoal. Nitrogen desorption at 77 K has been used to characterise the texture of the indicated activated specimen.

**2.4. Response Surface Methodology.** The Box-Behnken design includes specified placement of input parameters and has 3 dimensions for every element labelled as 1, 0, and +1. It was designed to predict a statistical approach and deliver high empirical results at the centre of a design project and lower at the frame's extremities. This is a rotational polynomial pattern with part of what makes up the centre point at the centre of the sides and even in the middle [23]. A Box-Behnken statistically exploratory approach using the RSM was employed to study the impacts of three variables: period, molar ratio, and temperatures. The responsive factors were selected as the iodine amount with methylene blue adsorbed. The Box-Behnken design was selected owing to its low cost and high efficiency [24, 25]. Experimentation results were recorded and then matched towards the two multiple regres-

sions utilising the Design Expert 13 programme to assess the importance of a dependent dimension.

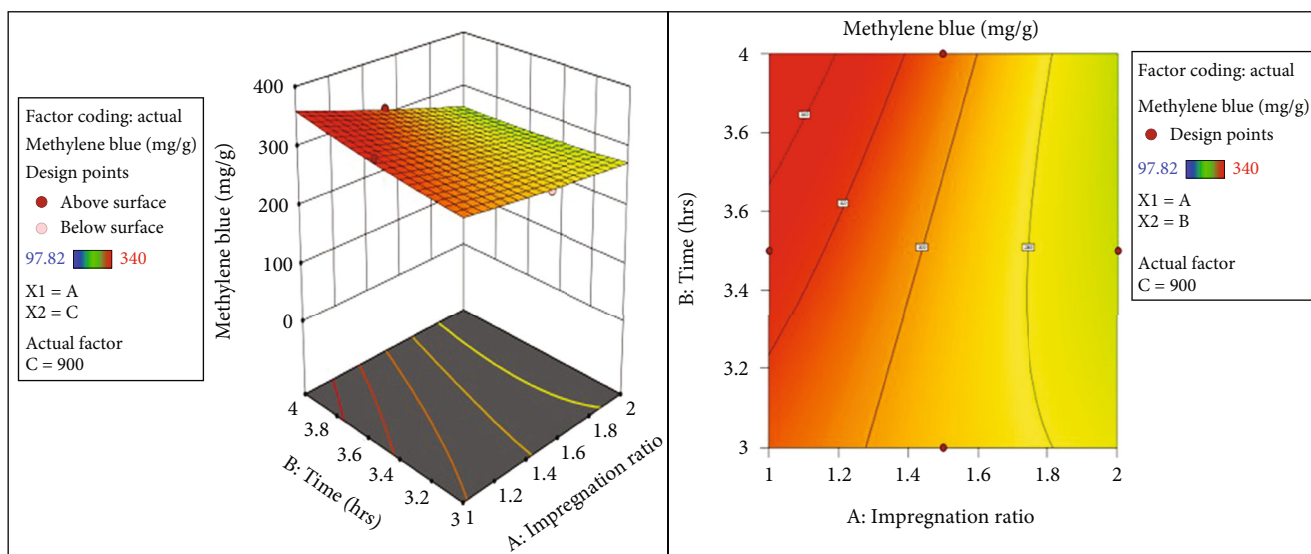
$$Z = A_0 + \sum_{i=1}^n A_i Y_i + \sum_{i=1}^n A_{ii} Y_i^2 + \sum_{i=1}^{n-1} A_{ij} Y_i Y_j + e. \quad (1)$$

$Z$  would be the appropriate reaction,  $Y_i$  and  $Y_j$  are the relevant factors,  $A_0$ ,  $A_i$ ,  $A_{ii}$ , and  $A_{ij}$  were predicted values for the interception, linearity, exponential, and interaction components,  $e$  is the errors, where  $n$  is the number of possibilities analysed. The  $F$  test was used to analyse the relevance of a functional form and its resulting consequences. The coefficient of determination  $R^2$  and modified  $R^2$  were used to measure the experience of the polynomial system of equations. The statistically significant correlation of a design was determined using variance analysis (ANOVA). The ideal parameters were determined using the following linear relationship; then, contours were utilised to examine every variable's interaction influence [26].

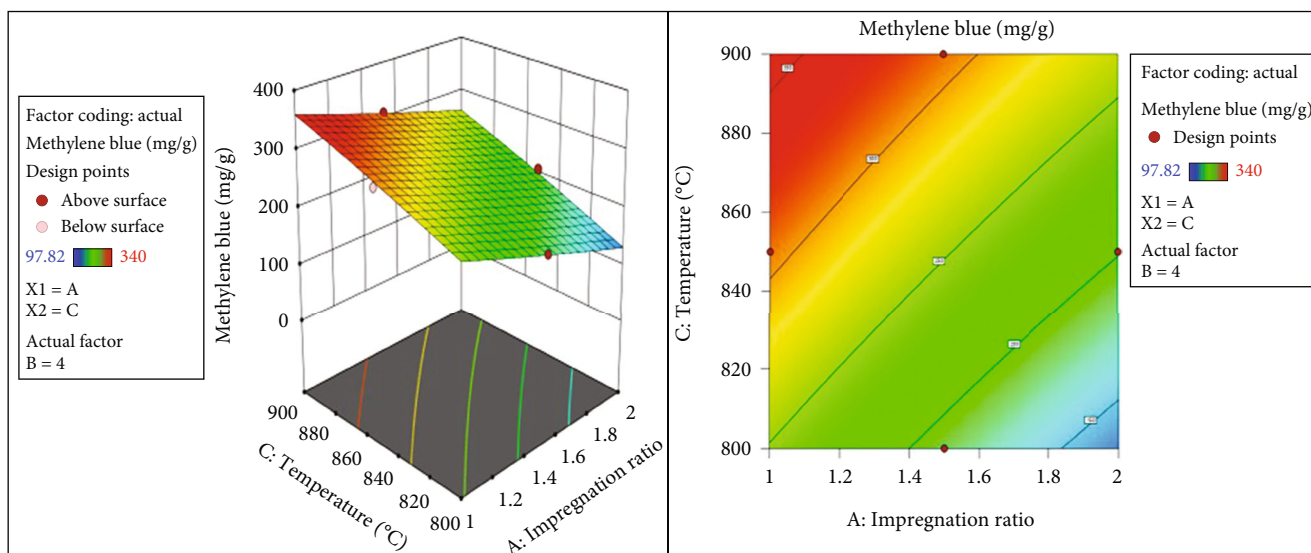
### 3. Result and Discussions

**3.1. RSM Models.** The Box-Behnken model is a helpful exploratory study using 3D surface methods based on 3 imperfect random effects. It aids in optimising the impacts of many factors, either solitary or interactive, to get the optimum results. The two elements in this concept are at the centre points of the processing satellite's borders and the centre. BBD is more effective for quadratic polynomials than orthogonal arrays (OA) and especially beneficial in preventing excessive control variables [27]. Table 1 shows the three critical parameters and the static loading with observable consequences of iodine. The absolute errors and variability were calculated using the cycle at the correct location. According to the



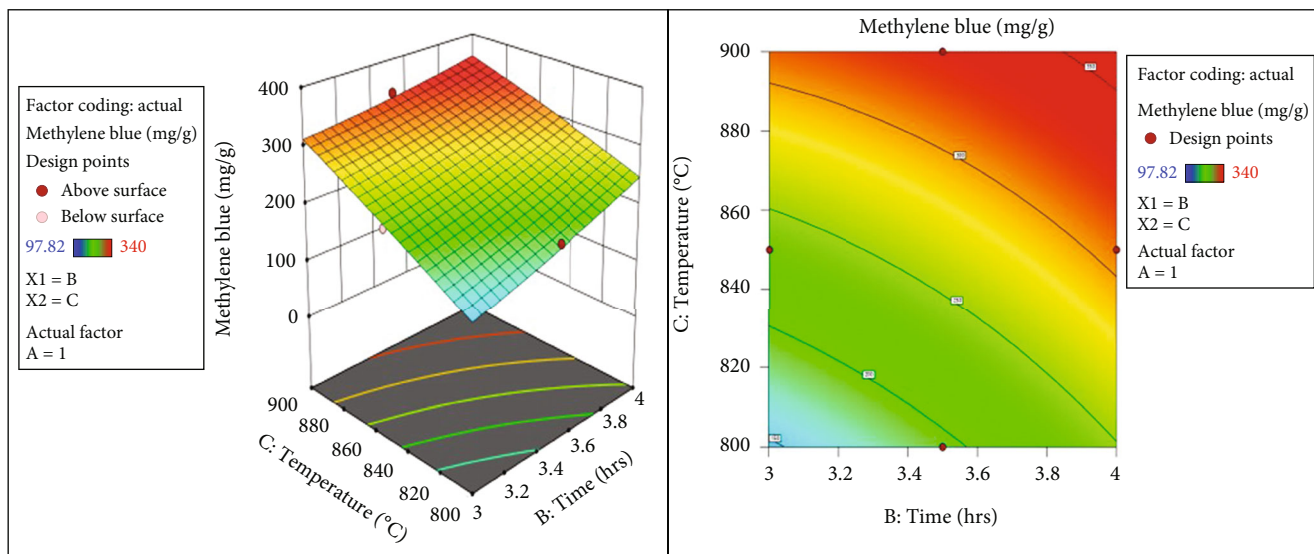


(a)



(b)

FIGURE 2: Continued.



(c)

FIGURE 2: Response 3D surface and contour plots of methylene blue based on the input parameters.

TABLE 2: ANOVA predictions of iodine number.

Source	SOS	Df	MS	F value	P value
Model	266749.359	9	29638.818	20.085	0.001
Impregnation ratio	10222.856	1	10222.856	6.928	0.034
Time	8020.301	1	8020.301	5.435	0.053
Temperature	234646.751	1	234646.751	159.012	0.001
AB	8649.651	1	8649.651	5.862	0.046
AC	339.112	1	339.112	0.230	0.646
BC	4626.040	1	4626.040	3.135	0.120
$\hat{A}^2$	36.794	1	36.794	0.025	0.879
$\hat{B}^2$	24.331	1	24.331	0.016	0.901
$\hat{C}^2$	183.709	1	183.709	0.124	0.735
Residual	10329.579	7	1475.654		
Lack of fit	5049.996	3	1683.332	1.275	0.396
Pure error	5279.583	4	1319.896		
Cor total	277078.938	16			

programme, the model equation was chosen for matching iodine and methylene blue adsorption abilities. After excluding the statistically irrelevant impacts of salt and methylene blue absorption, our final empirical regressors in terms of coding components were just as shown in the following:

$$\begin{aligned} \text{Iodine} = & 1059.26 - 35.75A + 31.66B + 171.26C + 46.50AB \\ & + 9.21AC + 34.01BC - 2.96A^2 + 2.96B^2 - 6.61C^2, \end{aligned} \quad (2)$$

$$\begin{aligned} \text{Methylene blue} = & 225.55 - 38.43A + 22.69B + 74.13C \\ & - 14.69AB + 4.82AC - 13.63BC \\ & + 1.94A^2 + 4.36B^2 - 3.76C^2. \end{aligned} \quad (3)$$

The measured results of iodine and methylene blue adsorbed were in excellent accordance with quantities anticipated by equations as shown in Figures 1 and 2. The corrected reliability ratio ( $R^2$ ) estimates for Equations (2) and (3) of the models remained at 0.9618 and 0.9793, correspondingly. All values of  $R^2$  are near 1.0, suggesting that the constructed regression analysis is very reliable in describing the variances in the empirical observations.

In the instance of iodine absorption values in Figures 1(a)–1(c), every linear regression graph exhibits a distinct peak along with symmetrically filled arcs in the associated contour showing that the peak amount of a reaction (Z1) is achievable inside the design process. Figures 2(a)–2(c) exhibit multiple (3D) linear regression graphs of a predicted quadratic polynomial for methylene blue adsorption, correspondingly. As

TABLE 3: ANOVA prediction of methylene blue.

Source	SOS	Df	MS	F value	P value
Model	61736.363	9	6859.596	41.736	0.001
Impregnation ratio	11812.614	1	11812.614	71.871	0.001
Time	4120.050	1	4120.050	25.068	0.002
Temperature	43956.125	1	43956.125	267.441	0.001
AB	862.891	1	862.891	5.250	0.056
AC	92.930	1	92.930	0.565	0.477
BC	742.563	1	742.563	4.518	0.071
AA <sup>2</sup>	15.794	1	15.794	0.096	0.766
BA <sup>2</sup>	80.105	1	80.105	0.487	0.508
CA <sup>2</sup>	59.550	1	59.550	0.362	0.566
Residual	1150.506	7	164.358		
Lack of fit	561.290	3	187.097	1.270	0.397
Pure error	589.216	4	147.304		
Cor Total	62886.869	16			

shown in Figures 2(a)–2(c), ignition delay has by far the most dramatic influence ( $F$  value = 41.73) on methylene blue (Y2) sorption of any three components tested (activating heat, molar ratio, and reaction rate). However, according to Figure 2(a), the combined impact of heating rate on iodine has no substantial effect on the growth of adsorbent values under the circumstances examined [28]. Figures 2(b) and 2(c) show that a prolonged incubation period is beneficial for increasing methylene blue adsorbent dosage.

The design project's desired spot predictions feature was used to figure out how to maximise the absorption coefficients of iodine and methylene blue within the experiment limits investigated. The projected best adhesion values were found by employing an activating temperature of 898.91°C, an impregnation ratio of 1.52, and an active duration of 3.5 hours. Considering the real-time operating procedure, the altered optimal conditions were determined as 900° C, impregnation ratio, and 3.5 hours. Adsorbent uptakes of iodine and methylene blue were determined to be 1247.63 mg/g and 340 mg/g, correspondingly. To validate the projected findings, several desorption specimens were created under the ideal conditions above for further iodine and methylene blue sorption experiments. The mean measurement results for iodine and methylene blue desorption were 1055.89 mg/g and 226.74 mg/g, correspondingly, which are in good accordance with econometric methods' impact on subsequent, having relatively little uncertainties of 1.56% and 1.80%, respectively. The operating parameters for the coagulant are detailed in Table 2.

A descriptive analysis (ANOVA) was used to assess the model's relevance and appropriateness and to discover the complicated link between factors and outcomes. Tables 2 and 3 summarise the presented iodine and methylene blue summary statistics. Due to the absence of fitting rates, estimated  $F$  values, and a very low probability for answers and values of  $P$  (0.001) as shown in Table 2, the regression has a firm fit and is considerable. Table 3 shows the ANOVA prediction of methylene blue.

Figures 3(a) and 3(b) show the normal probability plots of the outcomes of iodine and methylene blue. All Y12 interaction variables were found to be insignificant to the outcomes of the two experiments. Furthermore, the overall quadratic impacts of Y1 (temperature) and Y3 (time) are optimistic, indicating that these factors have a beneficial or cooperative influence on iodine and methylene blue desorption levels in the studied experimental location. Furthermore, the interaction factors Y1Y3 and Y2Y3, as well as Y2 and all exponential factors, show substantial as well as hostile impacts on reactions, meaning that increasing these variables further than the limitations is likely to lower iodine and methylene blue desorption levels.

For a successful fit, the endpoints must be near the fitting line, with small comfort intervals. Points just on the show's left or right, at the furthest average, have had the most leverage and can successfully drag the directly connected towards the centre [29, 30]. Exceptions are locations that are substantially distant from the line. All sorts of tips can degrade the fitting. The chart depicts an ANOVA analysis, but every piece of data is presented, giving readers far more information than simply the hypothesis. This standard error over the whole model range depicts the  $F$ -test, which indicates that almost all variables except for the slope are 0. The hypotheses test is practical when the standard error does not contain the horizontally neutral product lineup [31].

Jute inner carbon has iodine and methylene blue desorption capabilities of 846 mg/g and 98.21 mg/g, correspondingly. Those are all significantly less than all the carbonaceous materials generated under the given circumstances as shown in Figures 1 and 2. It was also found that the entire jute progenitor cell lump charcoal carbonised at 900°C for 3.5 hours had a methylene blue adsorption performance of 340 mg/g. As a result, adding an adequate weight ratio of potash bicarbonate to a substrate substantially influences the growth of the more expanded permeability inside the polymeric network. As the comparative temperature builds, the empirical model of both materials rises slowly, and a residual stress forms, indicating that the significant

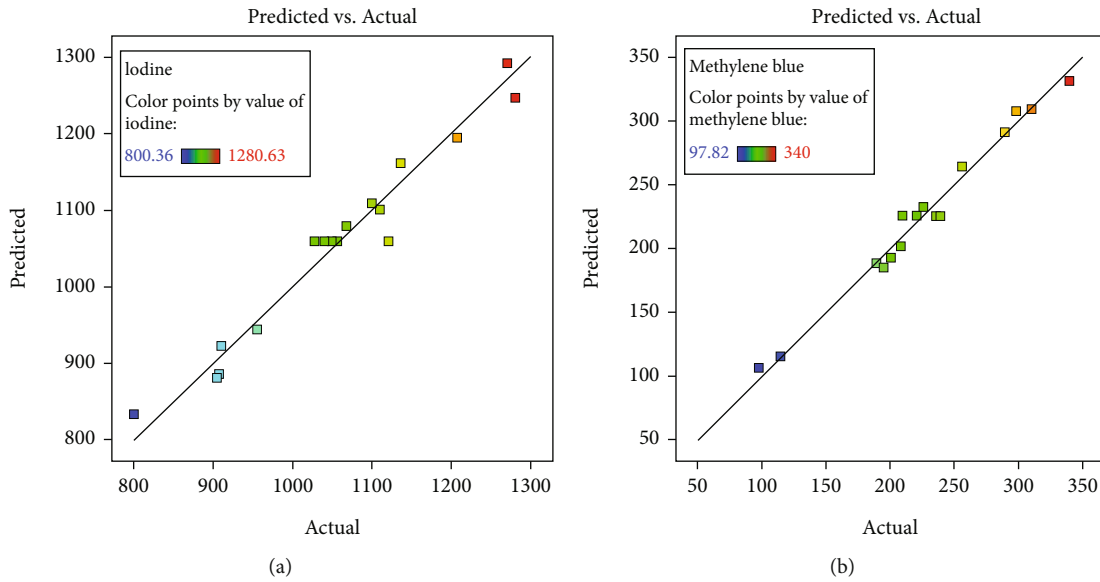


FIGURE 3: Actual vs. predicted plots of (a) iodine number and (b) methylene blue.

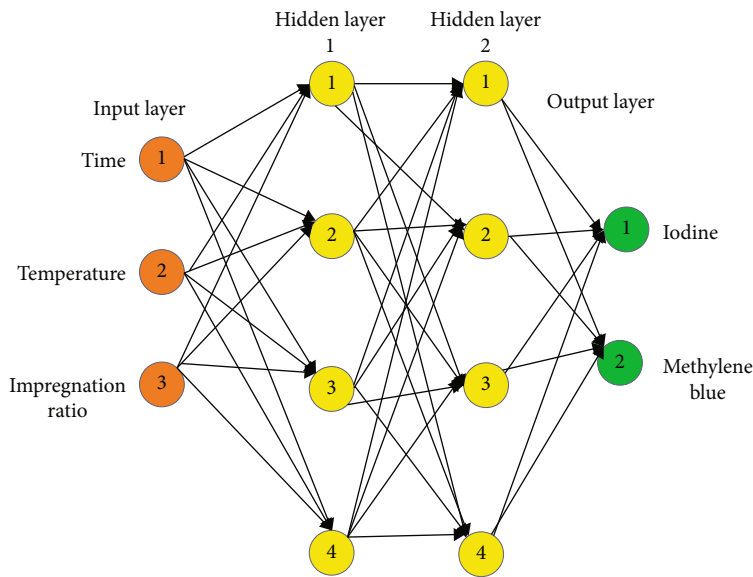


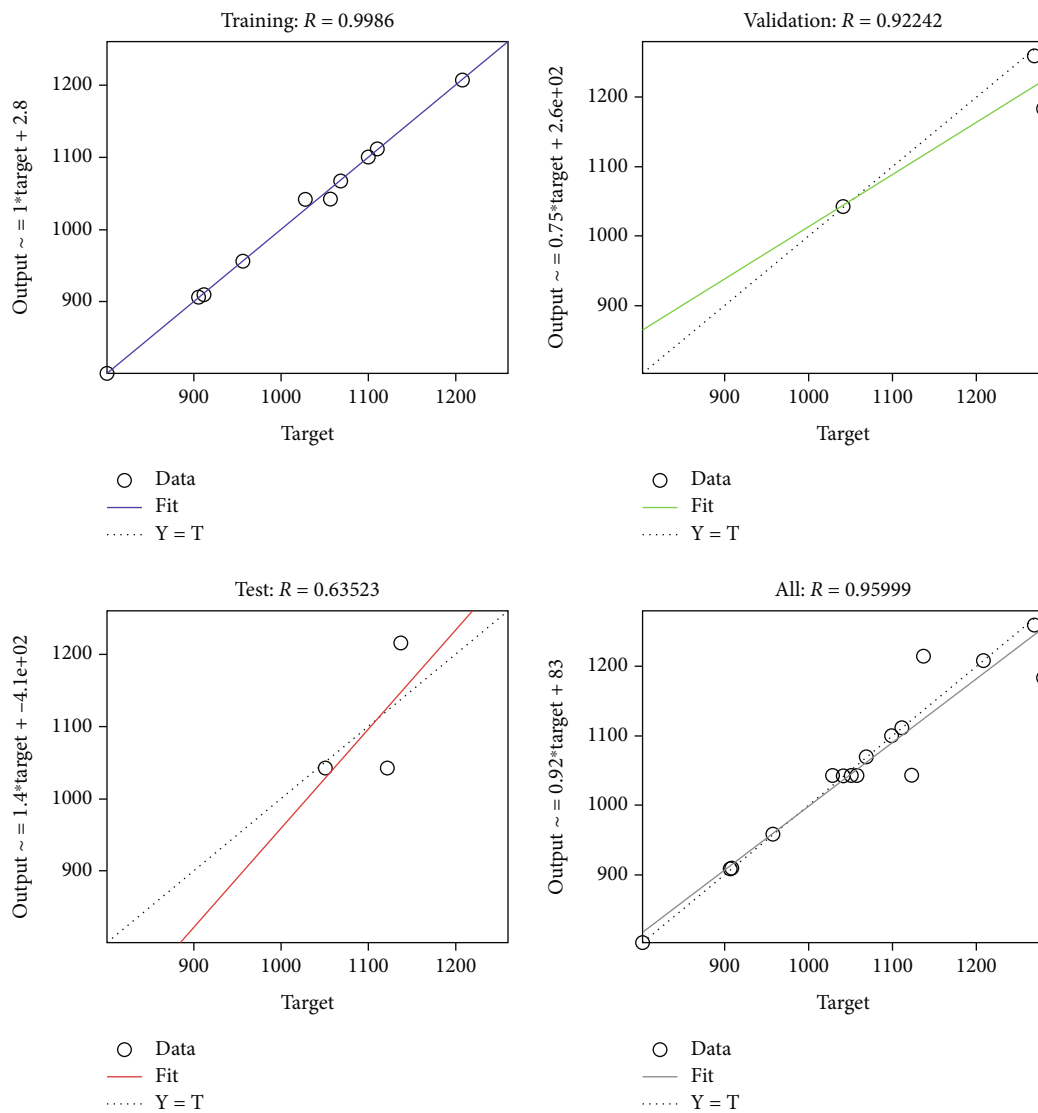
FIGURE 4: ANN structure of present research work.

number of small pores is linked with significant microporosity growth.

**3.2. Optimization through ANN Modelling.** In recent decades, ANN has emerged as a critical technique in the simulation and management of electrospun operations. As a computer tool, the ANN provides a graphical view with a slew of levels and multiple interacting processor parts that are primarily aware of inputs [32]. However, ANNs may adapt to real-world samples of a situation by utilising different equations among neurons and specialised machine learning built into the architecture of software applications. Figure 4 demonstrates the ANN structure of the current research.

The impregnation ratio, time length, and warmth were selected as input variables for the ANN, and the iodine number and methylene blue were selected as output results. This research explored the parabolic tangential, logistic digression, and linear activation parameters to improve the backpropagation neural network [33, 34]. Backpropagation (BP) has been used as a learning method to calculate performance gradients for weight vector parameter X. All specimens were separated into three subgroups at randomization to conduct an assessment. The supervised learning comprised 60% of specimens, the verification time series comprised 20% of specimens, and the testing data source held 20% of all specimens. The verification dataset is used to reduce the possibility of an over or forgetting [35]. This implies that whenever the inaccuracy of a





(a)

FIGURE 5: Continued.

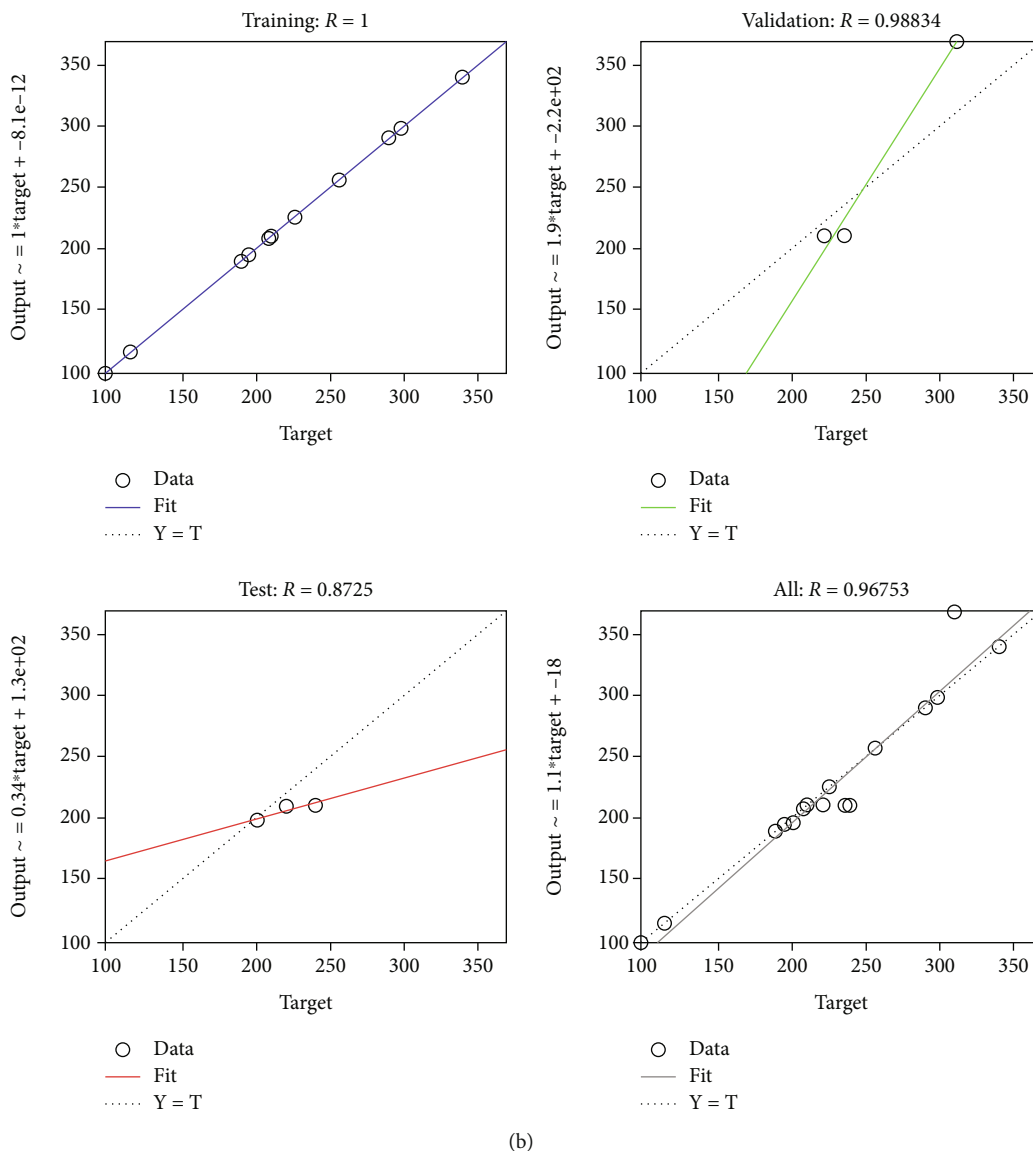


FIGURE 5: ANN performance features of (a) iodine number and (b) methylene blue.

learning test dataset drops while the fault of a testing dataset set grows, then network training is halted, and overtraining is prevented. Figures 5(a) and 5(b) show the predicted features of ANN results of iodine and methylene blue.

ANN can become caught in a minimum of errors, which the velocity factor helps to avoid. As a result, adopting the velocity factor reduces the probability of an under. This network can be trained using the Levenberg-Marquardt (LM) classification model. Although this approach handles general contour issues, its LM may be locked on the shortest path. To prevent the minimum error trapping, a velocity factor is provided. The Levenberg-Marquardt method is much more resilient than other algorithms that, in so many circumstances, result in the greatest network quality [36, 37]. A programme in MATLAB software was supplied to create the architecture of the graze and return network (version R2016). Since there is no predetermined procedure for determining its cortex and levels in the ANN framework,

the network output and stages are determined through experimentation. The number of nodes and levels was raised throughout this experiment to minimise the error function. Still, any growth in the population of neurons and levels did not improve the accuracy.

The assessment subcategories for training, validation, and assessment are shown in Table 4 along with the expected failure rate. Figures 5(a) and 5(b) show how well neurological systems predict what will happen. With values of 0.9599 for iodine and 0.9675 for methylene blue, the average amount of anticipated errors was reduced by less than 3%. Figures 6(a) and 6(b) are excellent instances of that one. Figures 7(a) and 7(b) provide iodine and methylene effectiveness graphs, respectively. The investigation was allowed since the measurement items were within the allowable levels. It can assess the accuracy of experiments conducted [38, 39]. The reliability of investigation, prediction, and artificial neural networks is summarised in Table 4.

TABLE 4: Predicted error based on the comparison of experimental and ANN values.

RUN	Experimental		ANN		Error	
	Iodine	Methylene blue	Iodine	Methylene blue	Iodine	Methylene blue
1	1182.650	340	1212.650	340	-2.53668	-3.00936E - 13
2	800.360	97.82	800.630	97.82	-0.03373	8.78917E - 12
3	1042.280	210	1072.280	210	-2.87831	-1.43462E - 12
4	1207.170	256.21	1201.250	256.21	0.490403	-1.17587E - 12
5	1068.250	298.19	1098.250	298.19	-2.80833	-6.67199E - 13
6	1100.287	225.79	1100.270	225.79	0.001545	-2.21543E - 12
7	1042.280	235.96	1042.000	210	0.026865	11.00186472
8	1042.280	239.65	1023.000	210	1.849791	12.37220947
9	1042.280	220.71	1072.280	210	-2.87831	4.852521408
10	1260.077	310.28	1290.077	369.2163412	-2.38081	-18.99456659
11	907.900	114.78	937.900	114.78	-3.30433	4.35809E - 12
12	910.650	200.89	910.580	197.0881454	0.007688	1.892505633
13	905.570	189.78	935.570	189.78	-3.31283	5.24165E - 13
14	956.170	194.89	956.320	194.89	-0.01569	0
15	1214.591	289.78	1248.210	289.78	-2.76793	-1.03965E - 12
16	1042.280	221.45	1165.320	210	-11.8049	5.170467374
17	1110.140	208.54	1040.140	208.54	6.305511	-4.77012E - 13

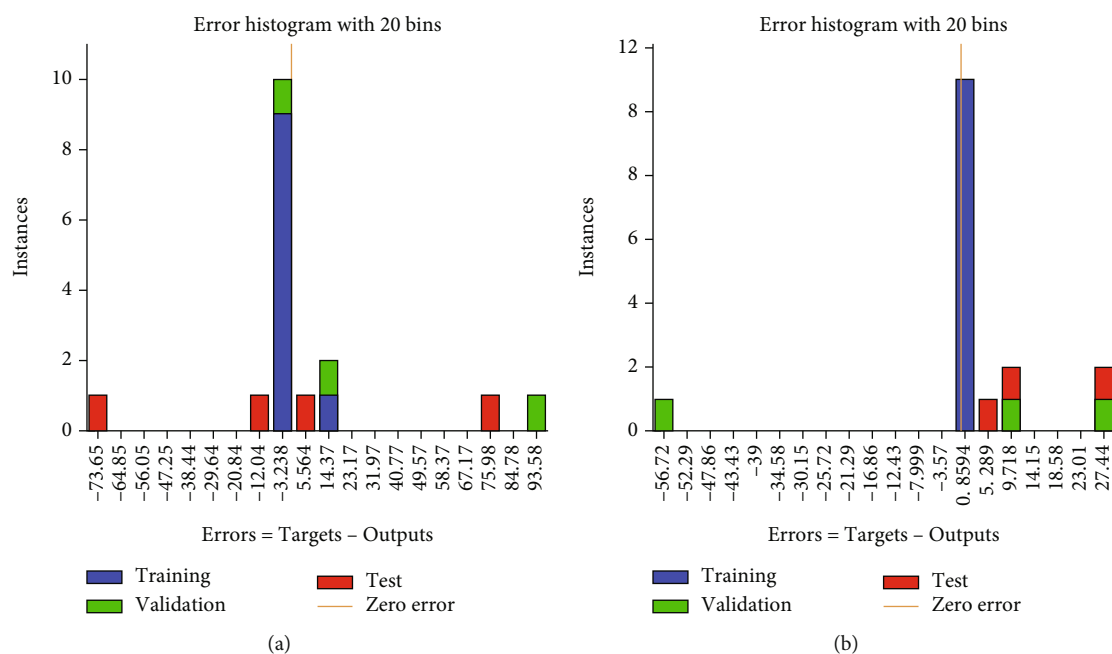


FIGURE 6: Error plots of (a) iodine and (b) methylene blue.

Statistical analysis revealed that the RSM or ANN approaches yield accurate findings.

According to the transmittance finding given in Figure 8, the adsorbed contains considerable microporous and mesoporous, compared with an average pore diameter of 3.16 nm. Comparison of experimental, RSM, and ANN-predicted values of iodine number and methylene blue are shown in Figures 8(a) and 8(b). Even though the precise emphasis given to  $K_2CO_3$  is unknown at the moment, given the crea-

tion of  $K_2C_3O_4$  just after evolvement with one additional molarity of CO at approximately 870°C, these same porous and papule responses begun by  $K_2CO_3$  stimulation might be temporarily posited to be quite comparable to an initiation action needed to make progress by  $K_2C_3O_4$  [40]. The additional CO launched during  $K_2CO_3$  dissolution, on either side, could act as a gas phase to aid in the removal of gasification volatile matter from the carbonaceous mixture to a high likelihood extent and have a moderate beneficial impact

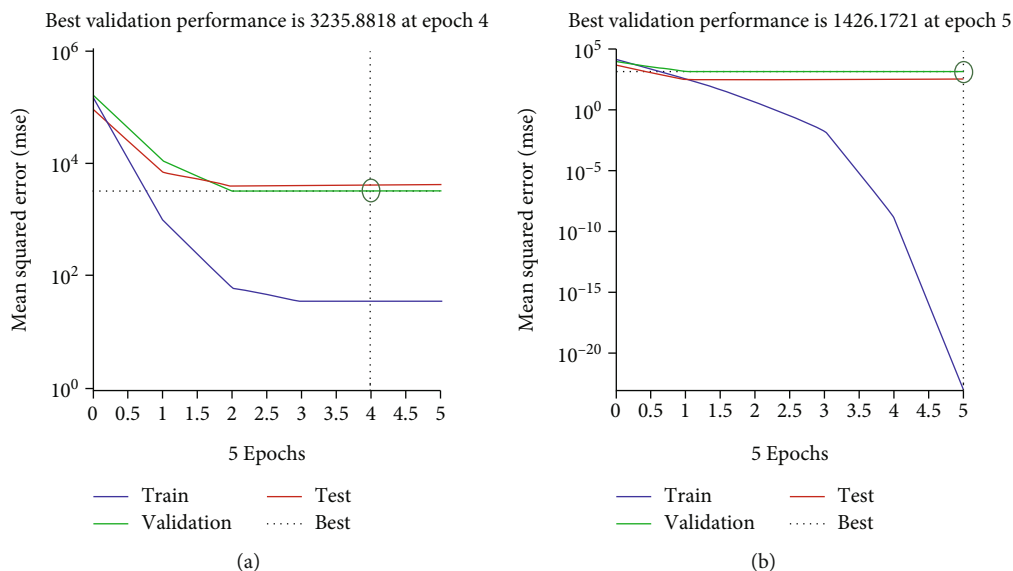


FIGURE 7: Effectiveness plots of (a) iodine and (b) methylene blue.

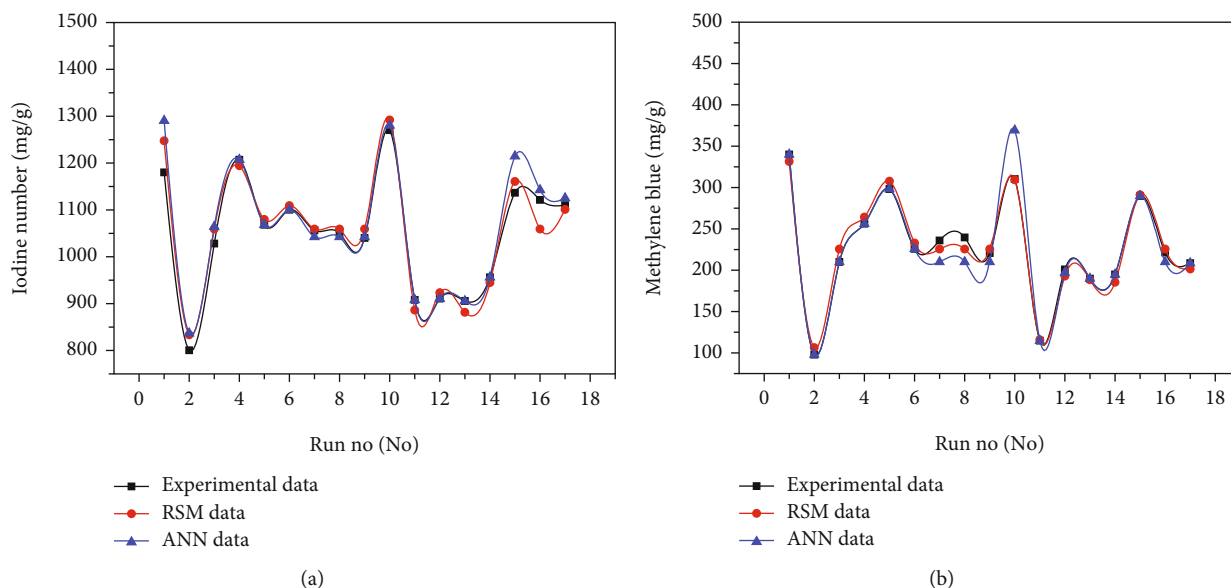


FIGURE 8: Comparison of experimental, RSM, and ANN-predicted values of (a) iodine number and (b) methylene blue.

on suppressing this same overaggressive porous broadening advancement to accomplish a relatively homogenous porous structure and high return [41]. Future studies should focus on a more in-depth examination of the activating effect of  $K_2CO_3$  and  $K_2C_3O_4$  on the pore structure of these carbonaceous materials. The ANN approach produced more future systems with a 95% reliability rate than response surface data. The ANN optimum model helps the user to account for the uncertainty associated with a particular cast combination.

#### 4. Conclusion

BBD effectively optimised the process of producing  $K_2CO_3$ -activated carbons from the jute core. RSM and ANN model-

ling were used to maximise the findings appropriately. The experimental results for iodine and methylene blue desorption were directly correlated very well with polynomial model predictions. The best charcoal was obtained using  $900^\circ C$  activating temperatures, a 1.5 molar ratio, and a 4-hour activating time. This resulted in iodine and methylene blue absorption of 1260.07 mg/g and 369.21 mg/g, respectively. It was discovered that the  $K_2CO_3$ -based pyrolysis process might be anticipated to become a safe yet incredibly efficient process of making activated carbons with a very well-defined and monocultural porous structure. Both the RSM and ANN models have to modify coefficients more significantly than 95%. (i.e.,  $R^2$  and adj.  $R^2$ ). The prediction of ANN values of 0.9599 for iodine and 0.9675 for methylene blue reduced the average amount of anticipated errors by

less than 3%. This clearly demonstrates that the adsorbed contains considerable microporous and mesoporous, compared with an average pore diameter of 3.16 nm. Even though the precise emphasis given to  $K_2CO_3$  is unknown at the moment, given the creation of  $K_2C_3O_4$  just after evolution with one additional molarity of CO at approximately 870°C, these same porous and papule responses begun by  $K_2CO_3$  stimulation might be temporarily posited to be quite comparable to an initiation action needed to make progress by  $K_2C_3O_4$ .

## Data Availability

The data used to support the findings of this study are included within the article. Should further data or information be required, these are available from the corresponding author upon request.

## Conflicts of Interest

The authors declare that there are no conflicts of interest regarding the publication of this paper.

## References

- [1] Y. Li and M. Zhang, "Mechanical properties of activated carbon fibers," *Activated Carbon Fiber and Textiles*, vol. 6, pp. 167–180, 2017.
- [2] I. Martin-Gullon and R. Font, "Dynamic pesticide removal with activated carbon fibers," *Water Research*, vol. 35, no. 2, pp. 516–520, 2001.
- [3] V. K. Gupta, D. Pathania, and S. Sharma, "Adsorptive remediation of Cu(II) and Ni(II) by microwave assisted  $H_3PO_4$  activated carbon," *Arabian Journal of Chemistry*, vol. 10, pp. S2836–S2844, 2017.
- [4] J. Zheng, Q. Zhao, and Z. Ye, "Preparation and characterization of activated carbon fiber (ACF) from cotton woven waste," *Applied Surface Science*, vol. 299, pp. 86–91, 2014.
- [5] C. Nieto-Delgado, D. Partida-Gutierrez, and J. R. Rangel-Mendez, "Preparation of activated carbon cloths from renewable natural fabrics and their performance during the adsorption of model organic and inorganic pollutants in water," *Journal of Cleaner Production*, vol. 213, pp. 650–658, 2019.
- [6] G. Velmurugan and K. Babu, "Statistical analysis of mechanical properties of wood dust filled jute fiber based hybrid composites under cryogenic atmosphere using Grey-Taguchi method," *Materials Research Express*, vol. 7, no. 6, 2020.
- [7] C. Ye, N. Hu, and Z. Wang, "Experimental investigation of *Luffa cylindrica* as a natural sorbent material for the removal of a cationic surfactant," *Journal of the Taiwan Institute of Chemical Engineers*, vol. 44, no. 1, pp. 74–80, 2013.
- [8] S. S. Munawar, K. Umemura, and S. Kawai, "Characterization of the morphological, physical, and mechanical properties of seven nonwood plant fiber bundles," *Journal of Wood Science*, vol. 53, no. 2, pp. 108–113, 2007.
- [9] M. C. Symington, W. M. Banks, O. D. West, and R. A. Pethrick, "Tensile testing of cellulose based natural fibers for structural composite applications," *Journal of Composite Materials*, vol. 43, no. 9, pp. 1083–1108, 2009.
- [10] R. Sudin and N. Swamy, "Bamboo and wood fibre cement composites for sustainable infrastructure regeneration," *Journal of Materials Science*, vol. 41, no. 21, pp. 6917–6924, 2006.
- [11] A. Kicińska-Jakubowska, E. Bogacz, and M. Zimmiewska, "Review of natural fibers. Part I—vegetable fibers," *Journal of Natural Fibers*, vol. 9, no. 3, pp. 150–167, 2012.
- [12] P. Gopinath, P. Murugesan, R. Manjula Devi et al., "Characterization of jute fibre-epoxy reinforced composites," *Materials Today: Proceedings*, vol. 46, pp. 8858–8863, 2021.
- [13] T. B. Yallem, P. Kumar, and I. Singh, "Sliding wear properties of jute fabric reinforced polypropylene composites," *Procedia Engineering*, vol. 97, pp. 402–411, 2014.
- [14] V. Ganesan and B. Kaliyamoorthy, "Utilization of Taguchi technique to enhance the interlaminar shear strength of wood dust filled woven jute fiber reinforced polyester composites in cryogenic environment," *Journal of Natural Fibers*, vol. 19, no. 6, pp. 1990–2001, 2022.
- [15] V. S. Chinta, P. Ravinder Reddy, and K. E. Prasad, "The effect of stacking sequence on the tensile properties of jute fibre reinforced hybrid composite material for axial flow fan blades: an experimental and finite element investigation," *Materials Today: Proceedings*, vol. 59, pp. 747–755, 2022.
- [16] A. K. Mohanty and M. Misra, "Studies on jute composites—a literature review," *Polymer-Plastics Technology and Engineering*, vol. 34, no. 5, pp. 729–792, 1995.
- [17] N. Reddy and Y. Yang, "Biofibers from agricultural byproducts for industrial applications," *Trends in Biotechnology*, vol. 23, no. 1, pp. 22–27, 2005.
- [18] A. K. Mohanty, M. A. Khan, and G. Hinrichsen, "Surface modification of jute and its influence on performance of biodegradable jute-fabric/Biopol composites," *Composites Science and Technology*, vol. 60, no. 7, pp. 1115–1124, 2000.
- [19] S. Kaliappan, S. Mohanamurugan, and P. K. Nagarajan, "Numerical investigation of sinusoidal and trapezoidal piston profiles for an IC engine," *Journal of Applied Fluid Mechanics*, vol. 13, no. 1, pp. 287–298, 2020.
- [20] J. Kazemi and V. Javanbakht, "Alginate beads impregnated with magnetic [email protected] nanocomposite for cationic methylene blue dye removal from aqueous solution," *International Journal of Biological Macromolecules*, vol. 154, pp. 1426–1437, 2020.
- [21] H. B. Quesada, T. P. de Araújo, L. F. Cusioli, M. A. S. D. de Barros, R. G. Gomes, and R. Bergamasco, "Caffeine removal by chitosan/activated carbon composite beads: adsorption in tap water and synthetic hospital wastewater," *Chemical Engineering Research and Design*, vol. 184, pp. 1–12, 2022.
- [22] B. Debnath, D. Haldar, and M. K. Purkait, "Environmental remediation by tea waste and its derivative products: a review on present status and technological advancements," *Chemosphere*, vol. 300, p. 134480, 2022.
- [23] V. Balaji, S. Kaliappan, D. M. Madhuvanesan, D. S. Ezhumalai, S. Boopathi, and S. Mani, "Combustion analysis of biodiesel-powered propeller engine for least environmental concerns in aviation industry," *Aircraft Engineering and Aerospace Technology*, vol. 94, no. 5, pp. 760–769, 2022.
- [24] O. S. Onyekwere, C. Odiakoase, and K. A. Uyanga, "Multi response optimization of the functional properties of rubber seed – shear butter based core oil using D-optimal mixture design," *Archives of Foundry Engineering*, vol. 17, no. 4, pp. 207–223, 2017.
- [25] R. Ghelich, M. R. Jahannama, H. Abdizadeh, F. S. Torknik, and M. R. Vaezi, "Central composite design (CCD)-response



- surface methodology (RSM) of effective electrospinning parameters on PVP-B-Hf hybrid nanofibrous composites for synthesis of HfB<sub>2</sub>-based composite nanofibers,” *Composites Part B: Engineering*, vol. 166, pp. 527–541, 2019.
- [26] R. Sasidharan and A. Kumar, “Response surface methodology for optimization of heavy metal removal by magnetic biosorbent made from anaerobic sludge,” *Journal of the Indian Chemical Society*, vol. 99, no. 9, article ???, 2022.
- [27] M. S. Bhatti, D. Kapoor, R. K. Kalia, A. S. Reddy, and A. K. Thukral, “RSM and ANN modeling for electrocoagulation of copper from simulated wastewater: multi objective optimization using genetic algorithm approach,” *Desalination*, vol. 274, no. 1-3, pp. 74–80, 2011.
- [28] S. J. Muthiya, L. Natrayan, S. Kaliappan et al., “Experimental investigation to utilize adsorption and absorption technique to reduce CO<sub>2</sub> emissions in diesel engine exhaust using amine solutions,” *Adsorption Science & Technology*, vol. 2022, article 9621423, pp. 1–11, 2022.
- [29] M. M. Matheswaran, T. V. Arjunan, S. Muthusamy et al., “A case study on thermo-hydraulic performance of jet plate solar air heater using response surface methodology,” *Case Studies in Thermal Engineering*, vol. 34, article 101983, 2022.
- [30] V. Paranthaman, K. Shanmuga Sundaram, and L. Natrayan, “Influence of SiC particles on mechanical and microstructural properties of modified interlock friction stir weld lap joint for automotive grade aluminium alloy,” *Silicon*, vol. 14, no. 4, pp. 1617–1627, 2022.
- [31] B. Subramanian, N. Lakshmaiya, D. Ramasamy, and Y. Devarajan, “Detailed analysis on engine operating in dual fuel mode with different energy fractions of sustainable HHO gas,” *Environmental Progress & Sustainable Energy*, vol. 41, no. 5, article e13850, 2022.
- [32] A. E. Rodríguez-Sánchez, E. Ledesma-Orozco, S. Ledesma, and A. Vidal-Lesso, “Application of artificial neural networks to map the mechanical response of a thermoplastic elastomer,” *Materials Research Express*, vol. 6, no. 7, 2019.
- [33] G. J. Yun, J. Ghaboussi, and A. S. Elnashai, “A new neural network-based model for hysteretic behavior of materials,” *International Journal for Numerical Methods in Engineering*, vol. 73, no. 4, pp. 447–469, 2008.
- [34] D. M. Dimiduk, E. A. Holm, and S. R. Niezgoda, “Perspectives on the impact of machine learning, deep learning, and artificial intelligence on materials, processes, and structures engineering,” *Innovations*, vol. 7, no. 3, pp. 157–172, 2018.
- [35] D. Wang, Q. Zhu, Z. Wei et al., “Hot deformation behaviors of AZ91 magnesium alloy: constitutive equation, ANN- based prediction, processing map and microstructure evolution,” *Journal of Alloys and Compounds*, vol. 908, p. 164580, 2022.
- [36] F. Masi and I. Stefanou, “Multiscale modeling of inelastic materials with thermodynamics-based artificial neural networks (TANN),” *Computer Methods in Applied Mechanics and Engineering*, vol. 398, article 115190, 2022.
- [37] A. Habib and U. Yildirim, “Developing a physics-informed and physics-penalized neural network model for preliminary design of multi-stage friction pendulum bearings,” *Engineering Applications of Artificial Intelligence*, vol. 113, p. 104953, 2022.
- [38] J. Du, Y. Wu, Z. Dong et al., “Single and competitive adsorption between indigo carmine and methyl orange dyes on quaternized kapok fiber adsorbent prepared by radiation technique,” *Separation and Purification Technology*, vol. 292, p. 121103, 2022.
- [39] D. Ghosh and K. G. Bhattacharyya, “Adsorption of methylene blue on kaolinite,” *Applied Clay Science*, vol. 20, no. 6, pp. 295–300, 2002.
- [40] M. Rafatullah, O. Sulaiman, R. Hashim, and A. Ahmad, “Adsorption of methylene blue on low-cost adsorbents: a review,” *Journal of Hazardous Materials*, vol. 177, no. 1-3, pp. 70–80, 2010.
- [41] V. S. Shankar, G. Velmurugan, S. Kaliappan et al., “Optimization of CO<sub>2</sub> concentration on mortality of various stages of *Callosobruchus maculatus* and development of controlled atmosphere storage structure for black gram grains,” *Adsorption Science & Technology*, vol. 2022, pp. 1–12, 2022.